Chinese Chemical Letters 37 (2026) 111916

Contents lists available at ScienceDirect

Chinese Chemical Letters

journal homepage: www.elsevier.com/locate/cclet

An optical pressure sensing phosphor of high-sensitivity by soft structure

Ruijing Fu[a,c], Bin Xiao[a], Haoyuan Weng[a], Pan Wang[a], Guangxia Wang[a,*], Qingguang Zeng[a,c,*], Dawei Wen[a,c,*], Guanjun Xiao[b,*]

[a] School of Applied Physics and Materials, Wuyi University, Jiangmen 529020, China
[b] State Key Laboratory of High Pressure and Superhard Materials, College of Physics, Jilin University, Changchun 130012, China
[c] Institute of Carbon Peaking and Carbon Neutralization, Wuyi University, Jiangmen 529020, China

ARTICLE INFO

Article history:
Received 24 July 2025
Revised 19 September 2025
Accepted 28 September 2025
Available online 29 September 2025

Keywords:
High pressure
Sr9Ga0.5(PO4)7:0.5Cr3+
High-pressure sensitivity
Optical pressure sensors
Low-dimensional structures

ABSTRACT

Luminescent materials function as optical pressure sensors based on pressure-dependent emission. Optical pressure sensors offer a broad measurement range and non-contact operation but face limitations in sensitivity. In this study, we establish a selection principle based on low-dimensional structures and conduct a high-pressure evaluation of xCr^{3+}-doped $Sr_9Ga_{1-x}(PO_4)_7$ (x = 0.2, 0.5, and 0.8) phosphor, demonstrating its exceptional pressure sensitivity. Upon excitation at 488 nm, $Sr_9Ga_{0.5}(PO_4)_7$:0.5Cr^{3+} displays a broad near-infrared emission peak centered at 840 nm. Specifically, the phosphor maintains its structural integrity under pressures up to 10.0 GPa, with a continuous blue shift. The fluorescence peak shifts from 839.5 nm to 757.9 nm, demonstrating a high-pressure sensitivity of 8.11 nm/GPa. These findings establish $Sr_9Ga_{0.5}(PO_4)_7$:0.5Cr^{3+} as a viable candidate for optical pressure sensor, thereby offering valuable insights into advancing optical sensor development through host selection.

© 2025 Published by Elsevier B.V. on behalf of Chinese Chemical Society and Institute of Materia Medica, Chinese Academy of Medical Sciences.

Pressure, as a fundamental physical parameter, plays a pivotal role in regulating the physicochemical characteristics of materials [1–5]. High pressure (HP) techniques provide an innovative approach for modulating electronic structures through continuously reducing the distances between atoms and altering the electron orbitals, resulting in the discovery of new materials with exceptional performance that cannot be achieved under ambient conditions [6–12]. Therefore, high pressure technology greatly broadens the research scope of material science, with applications spanning various fields, including geophysics, novel material synthesis, optoelectronic properties of materials, and superconductivity [13–19]. Moreover, the spectral characteristics of optical pressure sensors, which are luminescent materials doped with optically active lanthanide or transition metal ions, under pressure provide a deeper understanding of their luminescence mechanisms and expand their applications in fields such as pressure sensing [20–22]. This includes analyzing the shifts of excitation/emission spectra, changes of band intensity, and variations in the full width at half maximum (FWHM) of the spectra. Which are often utilized to detect pressure changes in the symmetric diamond anvil cells (DACs) [23,24]. Compared to visible light, near-infrared (NIR) radiation exhibits lower propagation losses and low scattering. Moreover, NIR spectroscopy has emerged as a versatile lighting and analytical tool, actively enabling applications in food analysis, plant growth, night vision, and biomedical imaging due to its invisibility to the human eye and its ability to be selectively absorbed by specific molecular bonds [25–27]. Cr^{3+} ions, characterized by their unique $3d^3$ electronic configurations, are prominent candidates for broadband NIR luminescence. This prominence stems from their high photoluminescence quantum yields (PLQYs), tunable emission wavelengths, and compatibility with efficient excitation by commercially available blue light-emitting diodes (LEDs) [28–32]. The luminescence properties of Cr^{3+} ions are influenced by both temperature and pressure, making them applicable for use in thermometry and pressure sensing, respectively. Currently, ruby crystal (Al_2O_3:Cr^{3+}) is typically used as an optical pressure sensor in high-pressure research. However, its application is limited by a low sensitivity ($|S|$) value of 0.365 nm/GP [33]. To solve this issue, more optical manometers were developed recently, which based on luminescent materials. For example, Zou *et al.* reported the $Ca_9NaZn(PO_4)_7$:1.0 %Eu^{2+} with a high $|S|$ of 5.21 nm/GPa from 1 atm up to ~16.48 GPa [34]. Furthermore, luminescent materials with high $|S|$ at 10.0 GPa have been developed, for instance, Du *et al.* designed a $Ca_2Gd_{7.76}Ce_{0.24}Si_6O_{26}$ phosphor with

* Corresponding authors.
E-mail addresses: wangguangxia1107@126.com (G. Wang), zengqg1979@126.com (Q. Zeng), ontaii@163.com (D. Wen), xguanjun@jlu.edu.cn (G. Xiao).

https://doi.org/10.1016/j.cclet.2025.111916
1001-8417/© 2025 Published by Elsevier B.V. on behalf of Chinese Chemical Society and Institute of Materia Medica, Chinese Academy of Medical Sciences.

outstanding pressure sensing properties, with an enormous red shift of the emission band of 3.00 nm/GPa, and a decreasing FWHM of ~ 2.45 nm/GPa [35]. Marciniak reported that a 2 % Cr^{3+}-doped $LiSiGeO_4$ sample exhibited a sensitivity of 3.63 nm/GPa [36]. In addition, inorganic phosphors maintain persistent sensing functionality under pressures exceeding 10.0 GPa. Although the exploration of different luminescent materials has enhanced pressure sensitivity, most previously developed optical pressure sensors exhibit broadband emission, which still presents limitations for the precise measurement of low pressures. Furthermore, the forbidden d-d transitions of Cr^{3+} lead to low absorption, thereby reducing the luminous intensity of the phosphor [37]. Therefore, it is crucial to develop phosphors with high precision, high sensitivity, and high stability.

It is known that the enhanced flexibility of the lattice improves the compressibility of the material, thereby amplifying the luminescence changes under high pressure, and ultimately increasing the sensitivity [38,39]. Specifically, for phosphate, the elevated valence of P^{5+} hinders the formation of corner-sharing $[PO_4]^{3-}$ tetrahedra and a three-dimensional (3D) rigid framework, indicating it is likely to form a low-dimensional, low-rigidity structure. Consequently, it is anticipated that pressure sensors with high sensitivity ($|S|$) can be identified among phosphates [40–42]. Besides the $|S|$, the emission wavelength of optical pressure sensors warrants further consideration. Although, elevated Cr^{3+} doping enhances host absorption efficiency; the emission intensity is often compromised *via* concentration quenching. Therefore, designing high-sensitivity optical pressure sensing Cr^{3+} doping phosphors still challenges. The flexible lattice structure of $Sr_9Ga(PO_4)_7$ mitigates the concentration quenching induced by Cr^{3+} through structural confinement, thereby enhancing luminescence efficiency [43].

Here, a series of $Sr_9Ga_{1-x}(PO_4)_7{:}xCr^{3+}$ ($x = 0.2$, 0.5 and 0.8) phosphors were synthesized to investigate of the effects Cr^{3+} doping on the structural stability and optical characteristics. Comprehensive *in situ* high pressure Raman spectroscopy confirmed the structure stability of all phosphors under compression, without phase transition. Notably, *in situ* high pressure photoluminescence (PL) experiment revealed pressure-induced blue shifts in the emission bands. Specifically, the $Sr_9Ga_{0.5}(PO_4)_7{:}0.5Cr^{3+}$ phosphors exhibited a significant blue shift, characterized by a pressure coefficient of $d\lambda/dp = 8.11$ nm/GPa. The large shift highlights its potential for pressure sensing applications. The experimental data combined with theoretical calculations collectively verify the promising application prospects of $Sr_9Ga_{1-x}(PO_4)_7{:}xCr^{3+}$ ($x = 0.2$, 0.5 and 0.8) phosphors in advanced optical pressure detection technologies.

Phase-pure polycrystalline samples of $Sr_9Ga_{1-x}(PO_{4)7}{:}xCr^{3+}$ ($x = 0.2$, 0.5 and 0.8) were synthesized *via* solid-state reaction, details provided in Supporting information. Fig. 1a and Fig. S1 (Supporting information) illustrate the crystal structure of $Sr_9Ga_{1-x}(PO_4)_7{:}xCr^{3+}$ ($x = 0.2$, 0.5 and 0.8) at ambient pressure and temperature. Among the total $Sr_9Ga_{1-x}(PO_{4)7}{:}xCr^{3+}$ ($x = 0.2$, 0.5 and 0.8) crystal structure, $[GaO_6]$ and $[CrO_6]$ octahedra arranged in layers and positioned at the vertices, as well as the centers of edges, faces, and bodies of the unit cell, which arrangement results in a highly dispersed distribution of octahedra throughout the crystal lattice. Due to the weak nature of the ionic Sr-O, Ga-O, and Cr-O bonds, the structural framework is considered to be primarily composed of $[PO_4]$ tetrahedra containing P-O covalent bonds. Meanwhile, the $[GaO_6]$ octahedron is connected to six P-O tetrahedra *via* shared vertices and is tightly enclosed by several Sr-O polyhedral, forming a rigid framework. Doping with Cr^{3+} ions helps to suppress concentration quenching due to the exchange effect at short distances between activators [44]. Thus, the effective spatial isolation between $[CrO_6]$ octahedra sufficiently suppresses nonradiative energy transfer, thereby significantly mitigating concentration quenching while enhancing luminescent efficiency [45]. This structural confinement effect has been unambiguously demonstrated by the PL spectra and Luminescence decay curves of $Sr_9Ga_{1-x}(PO_4)_7{:}xCr^{3+}$ ($x = 0.2$, 0.5 and 0.8) (Fig. S2 in Supporting information). While exceeding a Cr^{3+} dopant concentration of $x = 0.5$ quenches the emission intensity, it does not alter the spectral position of the emission peak. This confirms that Cr^{3+} ions, regardless of dopant concentration, consistently substitute only one crystallographic position in the $Sr_9Ga(PO_4)_7$ structure. These results collectively demonstrate that the doping concentration yields the optimal luminescent performance across all measured optical properties. To investigate in detail the phase structure and purity of the synthesized phosphors, the Rietveld refinements of the powder X-ray diffraction (P-XRD) data were performed for $Sr_9Ga_{1-x}(PO_4)_7{:}xCr^{3+}$ ($x = 0.2$, 0.5, and 0.8) (Fig. 1b and Fig. S3 in Supporting information). The recorded diffraction patterns showed no significant differences and matched well with the reference patterns for the $Sr_9Ga(PO_4)_7$ phase, indicating that all samples were pure phase. $Sr_9Ga_{1-x}(PO_4)_7{:}xCr^{3+}$ ($x = 0.2$, 0.5 and 0.8) is mainly composed of partially agglomerated spherical particles with a size of about 2–5 μm, and the elemental distribution in the energy-dispersive X-ray spectroscopy (EDS) is also homogeneous, further confirming the pure phase nature of the samples (Fig. 1c).

The normalized excitation and emission spectra of the $Sr_9Ga_{0.5}(PO_4)_7{:}0.5Cr^{3+}$ phosphors are shown in Fig. 1d Under the excitation of 485 nm, the phosphor $Sr_9Ga_{0.5}(PO_4)_7{:}0.5Cr^{3+}$ exhibits broadband NIR luminescence spanning from 700 nm to 1100 nm, with a peak emission at 840 nm. This luminescent behavior is ascribed to the spin-allowed $^4T_2$ (4F) → $^4A_2$ transition characteristic of Cr^{3+} ions in an octahedral coordination environment [46]. Fig. 1e and Fig. S4 (Supporting Information) display the temperature-dependent PL spectrum of the $Sr_9Ga_{0.5}(PO_4)_7{:}0.5Cr^{3+}$, over the temperature range from 77 K to 450 K under 485 nm excitation. The PL intensity decreases gradually with increasing temperature due to thermal quenching caused by non-radiative processes. At higher temperatures, electrons are more likely to reach the intersection between the ground and excited states and return to the ground state *via* non-radiative transitions. To further investigate the local electronic state of Cr^{3+}, electron paramagnetic resonance (EPR) measurements were performed. As shown in Fig. 1f, $Sr_9Ga_{1-x}(PO_4)_7{:}xCr^{3+}$ ($x = 0.2$, 0.5 and 0.8) exhibit a broad single peak at $g \approx 1.96$, which is a typical signature of isolated Cr^{3+} ions in an octahedral crystal field. The consistent peak position across concentrations indicates that the local coordination environment of Cr^{3+} remains largely unchanged. With increasing doping levels, the signal intensity rises significantly, reflecting a greater number of paramagnetic centers, while the slight line broadening suggests enhanced spin-spin interactions and increased lattice disorder due to Cr^{3+} substituting for Ga^{3+}. In addition, to achieve a more profound comprehension of the elemental composition of the designed samples, the representative X-ray photoelectron spectroscopy (XPS) spectra of $Sr_9Ga_{1-x}(PO_4)_7{:}xCr^{3+}$ ($x = 0.2$, 0.5, 0.8) were recorded and are shown in Fig. 2. They clearly exhibit characteristic photoelectron peaks corresponding to Sr 3d, Ga 2p, Cr 2p, O 1 s, and P 2 s core levels. With the significant increase of doping, the XPS peak position did not change significantly. Combine the PL spectra and the Rietveld XRD refinements, which clearly demonstrate that present predominantly as Cr^{3+} at Ga sites in $Sr_9Ga(PO_4)_7$ and the occupied lattice site was largely unaffected by the doping level.

To evaluate the potential of $Sr_9Ga_{1-x}(PO_4)_7{:}xCr^{3+}$ ($x = 0.2$, 0.5, 0.8) phosphors as fluorescence-based pressure sensors, the pressure dependence of PL spectra was investigated under high pressure. Figs. 3a-c present the normalized PL spectra measured over the pressure range of 1 atm to 10.0 GPa under 488 nm excitation. As evidenced by published data, the spin-allowed nature of oc-

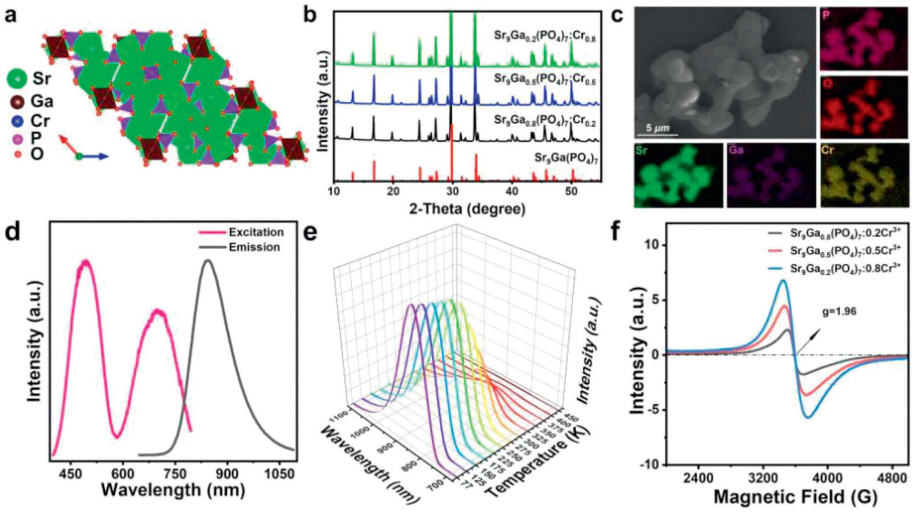


Fig. 1. (a) Crystal structure of $Sr_9Ga_{1-x}(PO_4)_7$:xCr^{3+} ($x = 0.2$, 0.5 and 0.8) along the *b* axis. (b) Powder XRD patterns of the synthesized $Sr_9Ga_{1-x}(PO_4)_7$:xCr^{3+} ($x = 0.2$, 0.5 and 0.8) phosphors. (c) SEM images and elemental mapping results of the $Sr_9Ga_{0.5}(PO_4)_7$:$0.5Cr^{3+}$. (d) Excitation and emission spectra of the $Sr_9Ga_{0.5}(PO_4)_7$:$0.5Cr^{3+}$ phosphor under excited 485 nm. (e) Temperature-dependent PL spectra at 77–500 K for $Sr_9Ga_{0.5}(PO_4)_7$:$0.5Cr^{3+}$. (f) The electron paramagnetic resonance spectroscopy of $Sr_9Ga_{0.5}(PO_4)_7$:$0.5Cr^{3+}$.

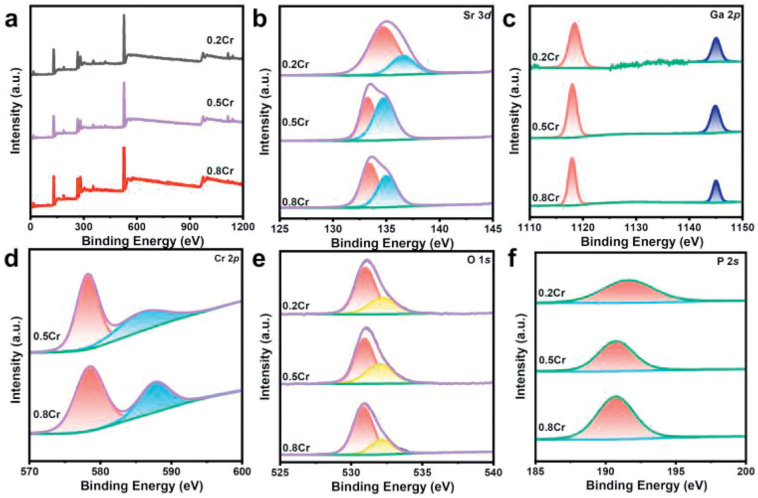


Fig. 2. (a) The XPS survey spectrum and XPS spectrum of the (b) Sr 3d, (c) Ga 2p, (d) Cr 2p, (e) O 1p, and (f) P 2p of $Sr_9Ga_{1-x}(PO_4)_7$:xCr^{3+} ($x = 0.2$, 0.5, 0.8).

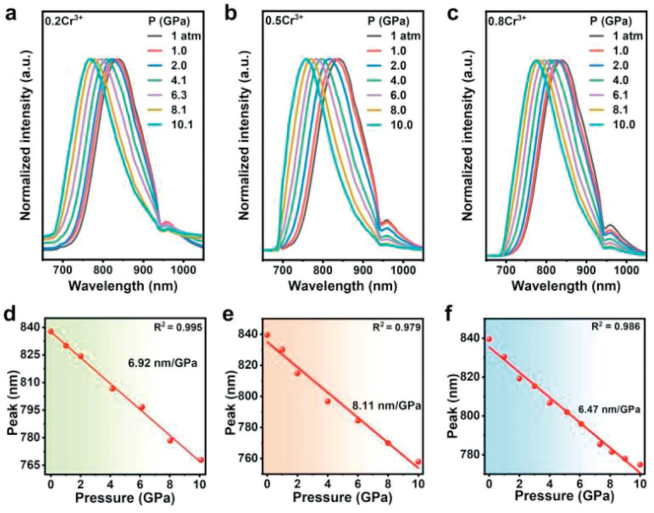


Fig. 3. (a-c) Normalized emission spectra and (d-f) corresponding peak position variation plots for the $Sr_9Ga_{0.8}(PO_4)_7$:$0.2Cr^{3+}$, $Sr_9Ga_{0.5}(PO_4)_7$:$0.5Cr^{3+}$ and $Sr_9Ga_{0.2}(PO_4)_7$:$0.8Cr^{3+}$ from 1 atm to 10.0 GPa.

tahedrally coordinated Cr^{3+} ions enable broad emission from the $^4T_2 \rightarrow {}^4A_2$ transition. However, for $Sr_9Ga(PO_4)_7$, the $^4T_2$ state invariably resides below the ^2E level, resulting in exclusive observation of broadband emission ($^4T_2 \rightarrow {}^4A_2$) while precluding detection of sharp line features ($^2E \rightarrow {}^4A_2$). As the pressure increases, it can be clearly seen that PL peak position is continuously blue shifted. Upon decompression, the peak position of PL spectrum can be restored to its original state (Fig. S5 in Supporting information), confirming its good stability and reversibility under extreme conditions. Meanwhile, we performed additional *in situ* high pressure PL experiments for the $Sr_9Ga_{0.8}(PO_4)_7$:$0.2Cr^{3+}$, $Sr_9Ga_{0.5}(PO_4)_7$:$0.5Cr^{3+}$and $Sr_9Ga_{0.2}(PO_4)_7$:$0.8Cr^{3+}$ from 1 atm to 10.0 GPa after three single compression-decompression cycles (Fig. S6 in Supporting information). The pressure-dependent PL spectra and the PL peak position are presented in Fig. S6. The repeated pressure cycles produced consistent photoluminescence behavior, supporting the reliability of phosphors as an optical pressure sensor. Throughout the entire process, each pressure point and the corresponding peak positions of the PL spectrum are illustrated in Figs. 3d-f. Notably, all xCr^{3+}-doped $Sr_9Ga_{1-x}(PO_4)_7$ phosphors exhibit systematic blue shifts under pressure, with concentration-dependent pressure coefficients of 6.08 nm/GPa

Table 1
Comparative analysis of pressure sensing capabilities in different luminescent materials emitting in the visible range utilized for optical manometry.

Luminescent materials	Sensitivity (nm/GPa)	Ref.
$Al_2O_3:Cr^{3+}$ (ruby)	0.365	[47,48]
$YAlO_3:Cr^{3+}$	0.70	[23]
$Sr_2LuNbO_6:Mn^{4+}$	0.82	[49]
$SrFCl:Sm^{2+}$	1.11	[50]
$Ca_4Y_3Si_7O_{15}N_5:Eu^{2+}$	1.13	[51]
$BaLi_2Al_2Si_2N_6:Eu^{2+}$	1.58	[52]
$Mg_2Gd_8(SiO_4)_6O_2:Ce^{3+}/Mn^{2+}$	1.84	[53]
$Lu_2Mg_2Al_2Si_2O_{12}:Eu^{2+}/Mn^{2+}$	3.53	[54]
$Ca_9NaZn(PO_4):Eu^{2+}$	5.21	[55]
$NaY_9(SiO_4)_6O_2:Mn^{2+}$	7.00	[56]
$Sr_9Ga_{0.5}(PO_4)_7:0.5Cr^{3+}$	8.11	This work
$Sr_8Si_4O_{12}Cl_8:Eu^{2+}$	9.69	[57]
$Li_3Sc_2(PO_4)_3:Cr^{3+}$	23.9	[58]

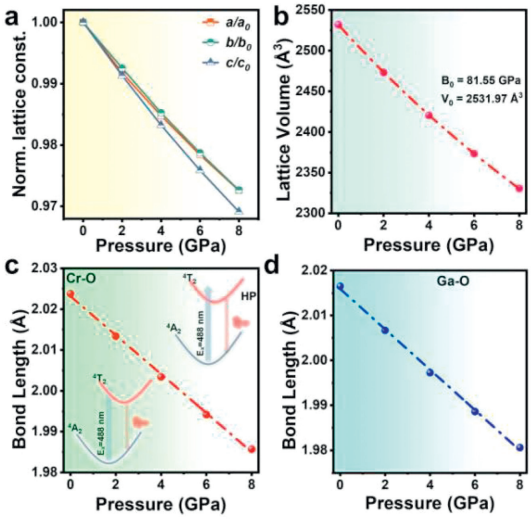


Fig. 4. (a, b) The bond length of Cr-O and Ga-O under different pressure. Tanabe-Sugano diagram under ambient and high pressure (HP), given in the inset. (c) Unit cell volume as a function of pressure. (d) Compressibility along different lattice axes.

($x = 0.2$), 8.11 nm/GPa ($x = 0.5$), and 6.47 nm/GPa ($x = 0.8$), indicating Ga-site occupancy modulates lattice compressibility. The superior pressure responsiveness of the $Sr_9Ga_{0.5}(PO_4)_7:0.5Cr^{3+}$ phosphors exhibits reversible and pressure-tunable luminescence, characterized by a systematic blue shift under hydrostatic compression. These pressure-induced spectral shifts. demonstrate significantly higher sensitivity (as quantified by the shift rates) than many reported phosphors under high pressure (Table 1). The composition-dependent shift rates highlight the role of Cr^{3+} concentration in modulating the pressure response. Specifically, $Sr_9Ga_{0.5}(PO_4)_7:0.5Cr^{3+}$ achieves a highest sensitivity (8.11 nm/GPa), surpassing numerous alternatives, this value remains below the highest-pressure sensitivity reported to date [23,47–58].

To elucidate the structural evolution of $Sr_9Ga_{0.5}(PO_4)_7:0.5Cr^{3+}$ in octahedral coordination environments, theoretical calculations and simulations were performed from 1atm to 8.0 GPa. The evolution of lattice constants and unit-cell volume with pressure is displayed in Figs. 4a and b. The distinct anisotropic compressibility can be observed, and the compressibility of the *c*-axis is higher than that of the *a* and *b* axis. The smaller ionic radius of Cr^{3+} ($R_{CrIII,6CN} = 0.615$ Å) compared to Ga^{3+} ($R_{GaIII,6CN} = 0.620$ Å) indicates that Cr-O bonds are shorter and stronger than Ga-O bonds [59]. Therefore, [GaO_6] octahedra are more easily compressed than [CrO_6] under increasing pressure. As we know, the luminescence properties of Cr^{3+} are strongly affected by the crystal field strength, which is governed by bond lengths. Therefore, the sensitivity of Cr^{3+} emission is related to the extent of increase or decrease in Cr-O bond lengths. Theoretical calculations reveal a shortening of both Cr-O and Ga-O bond lengths (Figs. 4c and d). Moreover, the [CrO_6] octahedra are well separated by [SrO_8] and [PO_4] polyhedra, and the minimum distance between adjacent [CrO_6] units is greater than 8.5 Å, which exceeds the typical distance (~5 Å) required for nonradiative energy transfer *via* exchange interaction. Meanwhile, the pressure evolution of the polyhedral [GaO_6] shows a trend towards structurally discontinuous distortion index during compression, and is dominated by the softer polyhedral [CrO_6], whose distortion index nearly doubles over the pressure range studied (Figs. S7a and b in Supporting information). This is the result of a continuous decrease in bond lengths Cr-O and Ga-O under compression. The decrease in bond length leads to an enhanced crystal field strength, resulting in a rise in the $^4T_2$ energy level of Cr^{3+} (inset of Fig. 4c) and a higher emission energy as explained by the Tanabe-Sugano diagram [60,61]. When the concentration of Cr^{3+} is low, most of the octahedra are [GaO_6], which absorb most of the external pressure through their compression. In this situation, the more rigid [CrO_6] octahedra share less of the pressure, resulting in reduced bond shortening and lower luminescence sensitivity to pressure. When the concentration of Cr^{3+} is very high, most of the octahedra are [CrO_6], which enhances the structural rigidity and bulk modulus. This also results in reduced bond shortening and lower luminescence sensitivity to pressure. This is further consistent with the blue shift in the PL spectra observed under increasing pressure (Figs. 3a-c).

The structural stability of $Sr_9Ga_{0.5}(PO_4)_7:0.5Cr^{3+}$ under high pressure was examined through pressure-dependent Raman spectroscopy. Fig. 5a presents a suite of Raman spectra covering an optical frequency range from 50 cm^{-1} to 1150 cm^{-1} under high pressure. At ambient conditions, the Raman spectrum for $Sr_9Ga_{0.5}(PO_4)_7:0.5Cr^{3+}$ has seven dominant bands initially located around ~285, 420, 454, 555, 585, 627, 962 cm^{-1}. As pressure increases, the Raman peaks toward higher wavenumbers during compression (Figs. 5b and c), which is associated with bond shortening under high pressure. Meanwhile, the linear fitting indicates that the initial centers of the Raman peaks shift at rates of 3.93, 1.84, 2.42, 1.02, 1.91, 2.32, and 4.69 cm^{-1}/GPa for peak at 256, 420, 454, 555, 589, 627, and 962 cm^{-1} respectively. In the wavenumber range of 950–990 cm^{-1}, isolated phosphate ions exhibit symmetric P-O stretching vibrations. Within the range of 1000–1175 cm^{-1}, the triply degenerate asymmetric P-O stretching modes appear, while the doubly degenerate bending modes and triply degenerate bending modes correspond to the O-P-O bending deformations of the tetrahedron, generating bands at 400–490 cm^{-1} and 550–635 cm^{-1}, respectively. Additionally, the bands below 370 cm^{-1} are attributed to external modes, likely arising from translational and rotational oscillations of phosphate groups, Sr, and Ga units. Importantly, the structure of the material can be restored to its original state during decompression, as evidenced by the Raman spectrum measured during the pressure release cycle. These findings demonstrate that the developed luminescent material is structurally stable under high pressure and exhibits fully reversible compression, making it suitable for optical load measurement applications.

Meanwhile, to systematically evaluate the chemical stability of $Sr_9Ga_{0.5}(PO_4)_7:0.5Cr^{3+}$, were immersed in aqueous (pH ≈ 7), acidic (0.1 mol/L HCl, pH ≈ 1), and alkaline (0.1 mol/L NaOH, pH ≈ 13) environments for isochronal aging tests. Under equivalent immersion durations, the phosphor exhibited high stability in aqueous media, retaining > 98 % of its initial luminescence intensity (Fig. 6). Acidic

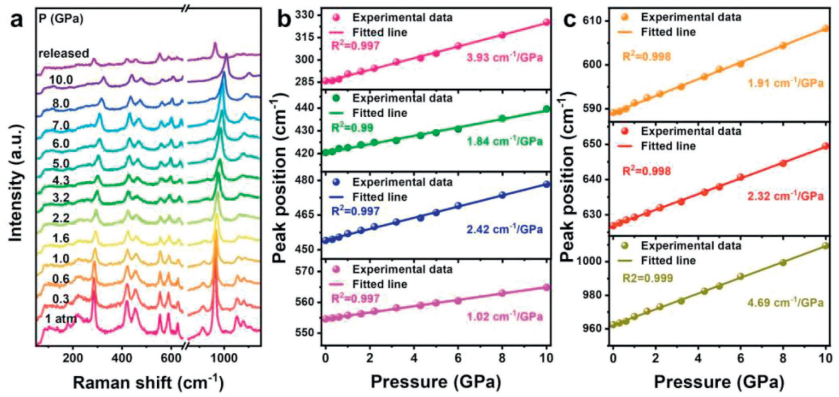


Fig. 5. (a) The pressure-dependent Raman spectra and (b, c) the determined peak for the $Sr_9Ga_{0.5}(PO_4)_7$:0.5Cr^{3+} phosphor as a function of pressure.

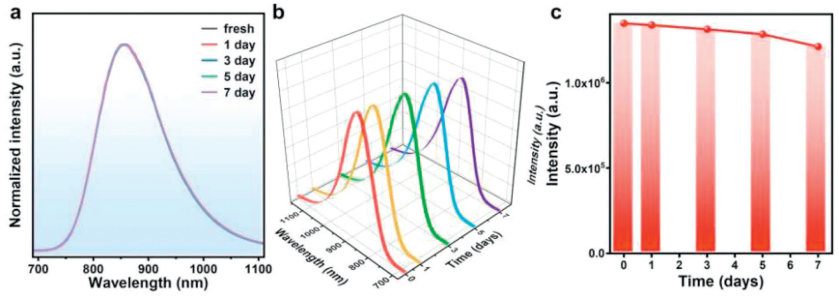


Fig. 6. The environmental stability characterization of $Sr_9Ga_{0.5}(PO_4)_7$:0.5Cr^{3+} phosphors under aqueous immersion (pH ≈ 7) after a week exposure.

conditions induced approximately 15 % intensity attenuation, while alkaline exposure triggered complete fluorescence quenching (Fig. S8 in Supporting information). The decomposition of $Sr_9Ga(PO_4)_7$ follows the chemical equilibrium below:

$$Sr_9Ga(PO_4)_7 \rightarrow 9Sr^{2+} + Ga^{3+} + 7PO_4^{3-} \quad (1)$$

In an alkaline solution, the electrostatic attraction between OH^- and cations (Sr^{2+} and Ga^{3+}) leads to the formation of insoluble hydroxides, causing cation loss from the solution. This strongly shifts the equilibrium toward the decomposition of $Sr_9Ga(PO_4)_7$, resulting in luminescence quenching. Conversely, in an acidic environment, H^+ interacts with the H^+ interacts with PO_4^{3-} to form soluble species (*e.g.*, $H_2PO_4^{2-}$, $H_2PO_4^-$, and H_3PO_4). These weakly shift the equilibrium toward decomposition, as PO_4^{3-} may be re-released into the solution. The decomposition of $Sr_9Ga(PO_4)_7$ in an alkaline and acidic solution follows the chemical equilibrium below:

$$Sr_9Ga(PO_4)_7 + 21OH^- \rightarrow 9Sr(OH)_2 + Ga(OH)_3 + 7PO_4^{3-} \quad (2)$$

$$Sr_9Ga(PO_4)_7 + 21H^+ \rightarrow 9Sr^{2+} + Ga^{3+} + 7H_3PO_4 \quad (3)$$

In addition, the XRD of $Sr_9Ga_{0.5}(PO_4)_7$:0.5Cr^{3+} phosphors for the pre- *vs* post-immersion under the three conditions are shown in Fig. S9 (Supporting information). The peak positions in both XRD and Raman spectra, although a reduction in peak intensity was consistently detected. The results indicate that the intensity loss arise from bulk decomposition and surface degradation. Furthermore, correlating with prior high-pressure characterization data, this material demonstrates not only structural stability under compression (≤10.0 GPa) but also exceptional aqueous-phase tolerance. These findings establish a critical physicochemical foundation for its deployment as a submersible pressure-sensing probe.

In conclusion, a novel optical pressure sensor $Sr_9Ga_{0.5}(PO_4)_7$:0.5Cr^{3+} phosphor has been successfully synthesized *via* the solid-state reaction, which exhibits a high sensitivity with $d\lambda/dP = 8.11$ nm/GPa under high pressure. Which because that Cr^{3+} substitution for Ga^{3+} further enhance the structural rigidity, suppressing non-radiative transitions and enabling high sensitivity of luminescence to both temperature and pressure. Specially, under pressures up to 10.0 GPa, the $Sr_9Ga_{0.5}(PO_4)_7$:0.5Cr^{3+} phosphor retains its phase structure, thereby showcasing excellent high-pressure stability. Meanwhile, the consistent photoluminescence behavior observed under repeated pressure cycles further affirms the material's suitability for application as an optical pressure sensor with pressure up to 10.0 GPa. This study demonstrates the dual functionality of $Sr_9Ga_{0.5}(PO_4)_7$:0.5Cr^{3+} as a luminescent material for pressure sensing under extreme conditions. Furthermore, it underscores the critical role of understanding high-pressure structural and luminescent behavior for advancing practical applications.

Declaration of competing interest

The authors declare that they have no known competing financial interests or personal relationships that could have appeared to influence the work reported in this paper.

CRediT authorship contribution statement

Ruijing Fu: Writing – original draft, Visualization, Conceptualization. **Bin Xiao:** Validation, Methodology, Data curation. **Haoyuan Weng:** Methodology, Data curation. **Pan Wang:** Methodology. **Guangxia Wang:** Supervision, Funding acquisition. **Qingguang Zeng:** Validation, Supervision, Funding acquisition, Conceptualization. **Dawei Wen:** Writing – review & editing, Supervision. **Guanjun Xiao:** Supervision, Funding acquisition.

Acknowledgments

This work was supported by National Natural Science Foundation of China (Nos. 12404024, 12174144, 12474009), Natural

Science Foundation of Guangdong Province (Nos. 2023A1515012706, 2022A1515011669), Open Project of State Key Laboratory of Superhard Materials, Jilin University (No.202414), Cooperative education platform of Guangdong Province (No. (2016) 31), Basic and Applied Basic Research Foundation of Jiangmen (No. 2020030102940008548), the Science Foundation for High-level Talents of Wuyi University (Nos. 2021AL019, 2019AL029).

Supplementary materials

Supplementary material associated with this article can be found, in the online version, at doi:10.1016/j.cclet.2025.111916.

References

[1] B. Li, K. Bian, X. Zhou, et al., Sci. Adv. 3 (2017) e1602916.
[2] T. Han, P. Gao, R. He, et al., J. Light Scatt. 34 (2022) 209–214.
[3] B. Li, X. Wen, R. Li, et al., Nat. Commun. 5 (2014) 4179.
[4] J. Liu, L. Zhang, B. Wu, et al., J. Light Scatt. 35 (2023) 1–7.
[5] G. Xiao, Y. Wang, D. Han, et al., J. Am. Chem. Soc. 140 (2018) 13970–13975.
[6] W. Zhao, G. Xiao, B. Zou, Aggregate 5 (2024) e461.
[7] Q. Li, Z. Chen, B. Yang, et al., J. Am. Chem. Soc. 142 (2020) 1786–1791.
[8] Z. Ma, F. Li, L. Sui, et al., Adv. Opt. Mater. 8 (2020) 2000713.
[9] Z. Ma, Z. Liu, S. Lu, et al., Nat. Commun. 9 (2018) 4506.
[10] Y. Shi, Z. Ma, D. Zhao, et al., J. Am. Chem. Soc. 141 (2019) 6504–6508.
[11] L. Zhang, L. Wu, K. Wang, et al., Adv. Sci. 6 (2019) 1801628.
[12] Z. Ma, F. Li, D. Zhao, et al., CCS Chem. 2 (2020) 71–80.
[13] D. Portehault, I. Gómez-Recio, M.A. Baron, et al., Chem. Soc. Rev. 51 (2022) 4828–4866.
[14] M. Xu, Y. Li, Y. Ma, Chem. Sci. 13 (2022) 329–344.
[15] B. Farhadi, D. Zheng, L. Liu, et al., Small Struct 5 (2024) 2300328.
[16] T. Hung, C. Huang, L. Deng, et al., Nat. Commun. 12 (2021) 5436.
[17] M. Cong, D. Zhao, J. Yang, et al., Research 7 (2024) 0476.
[18] M. Wang, Z. Ma, S. Li, et al., CCS Chem. (2025), doi:10.31635/ccschem.025.202505738.
[19] W. Zhao, J. Zhang, Z. Sun, et al., CCS Chem. 7 (2025) 1250–1271.
[20] H. Arashi, M. Ishigame, Japanese J. Appl. Phys. 21 (1982) 1647.
[21] A. Katrusiak, Acta Cryst. 75 (2019) 918–926.
[22] R. Keçili, S. Büyüktiryaki, İ. Dolak, et al., TrAC Trends Anal. Chem. 127 (2020) 115893.
[23] F. Datchi, A. Dewaele, P. Loubeyre, et al., High Pressure Res 27 (2007) 447–463.
[24] S. Kobyakov, A. Kamińska, A. Suchocki, et al., Appl. Phys. Lett. 88 (2006) 234102.
[25] M. Saleem, D. Varshney, J. Alloy. Compd. 708 (2017) 397–403.
[26] S. Wieghold, Y. Luo, A.S. Bieber, et al., Chem. Mater. 33 (2021) 6099–6107.
[27] R. Mahajan, R. Prakash, J. Mater. Sci.: Mater. Electron. 33 (2022) 25491–25517.
[28] B. Malysa, A. Meijerink, W. Wu, et al., J. Lumin. 190 (2017) 234–241.
[29] Q. Shao, H. Ding, L. Yao, et al., Opt. Lett. 43 (2018) 5251–5254.
[30] X. Xu, Q. Shao, L. Yao, et al., Chem. Eng. J. 383 (2020) 123108.
[31] L. Yao, Q. Shao, X. Xu, et al., Ceram. Int. 45 (2019) 14249–14255.
[32] L. Zhang, D. Wang, Z. Hao, et al., Adv. Optical Mater. 7 (2019) 1900185.
[33] F.D. Cortes-Vega, W. Yang, J. Zarate-Medina, et al., J. Am. Ceram. Soc. 102 (2019) 976–980.
[34] D. Zhang, B. Zheng, Z. Zheng, et al., Chem. Eng. J. 431 (2022) 133805.
[35] T. Zheng, L. Luo, P. Du, et al., Chem. Eng. J. 443 (2022) 136414.
[36] M. Szymczak, M. RunowskI, M.G. Brik, et al., Chem. Eng. J. 466 (2023) 143130.
[37] J.J. He, S.Y. Wu, L.J. Zhang, et al., J. Non-Cryst. Solids 437 (2016) 58–63.
[38] L. Lu, X. Wu, Z. Ji, et al., J. Aerosol Sci. 127 (2019) 18–26.
[39] I.Y. Chang, K. Hyeon-Deuk, ACS Appl Nano Mater 6 (2023) 9670–9678.
[40] G. Fan, H. Zhang, D. Fan, et al., Dalton Trans. 50 (2021) 13112–13123.
[41] H.J. Jessen, T. Dürr-Mayer, T.M. Haas, et al., Acc. Chem. Res. 54 (2021) 4036–4050.
[42] B. Malysa, A. Meijerink, T. Jüstel, Opt. Mater. 85 (2018) 341–348.
[43] F. Zhao, H. Cai, Z. Song, et al., Chem. Mater. 33 (2021) 3621–3630.
[44] Q. Shao, H. Ding, L. Yao, et al., RSC Adv. 8 (2018) 12035–12042.
[45] Z. Xia, G. Liu, J. Wen, et al., J. Am. Chem. Soc. 138 (2016) 1158–1161.
[46] S. Liu, Z. Wang, H. Cai, et al., Inorg. Chem. Front. 7 (2020) 1467–1473.
[47] J.D. Barnett, S. Block, G.J. Piermarini, Rev. Sci. Instrum. 44 (1973) 1–9.
[48] H.K. Mao, J. Xu, P.M. J. Geophys. Res. 91 (1986) 4673–4676.
[49] Z. Chen, S. Du, K. Zhu, et al., ACS Appl. Mater. Interfaces 15 (2023) 28193–28203.
[50] B. Lorenz, Y.R. Shen, W.B. Holzapfel, High Pressure Res. 12 (1994) 91–99.
[51] B. Zheng, Y. Song, Z. Zheng, et al., Inorg. Chem. 62 (2023) 4361–4372.
[52] Y. Wang, T. Seto, K. Ishigaki, et al., Adv. Funct. Mater. 30 (2020) 2001384.
[53] B. Zheng, X. Zhang, D. Zhang, et al., Chem. Eng. J. 427 (2022) 131897.
[54] D. Zhang, B. Zheng, Z. Zheng, et al., Chem. Eng. J. 431 (2022) 133805.
[55] Q. Zeng, M. Runowski, J. Xue, et al., Adv. Sci. 11 (2024) 2308221.
[56] T. Zheng, M. Runowski, J. Xue, et al., Adv. Funct. Mater. 33 (2023) 2214663.
[57] Z. Zheng, Y. Song, B. Zheng, et al., Inorg. Chem. Front. 10 (2023) 2788–2798.
[58] M. Szymczak, J. Jaśkielewicz, M. Runowski, et al., Adv. Funct. Mater. 34 (2024) 2314068.
[59] R.D. Shannon, Acta Cryst. 32 (1976) 751–761.
[60] D. Wen, H. Liu, Y. Guo, et al., Angew. Chem. Int. Ed. 61 (2022) e202204411.
[61] Y. Tanabe, S. Sugano, J. Phys. Soc. Jpn. 9 (1954) 766–779.